shown in Figure 7. The figure shows a single bias valence band (surface-to-tip) image where the four different selenium sites are easier to distinguish owing to the higher quality of the images obtained at a single bias.[11] The subsurface Re atom positions can be inferred by comparison with Figures 3 and 5b. These positions correspond to regions of intermediate tunneling current between the brightest areas, associated with the selenium atoms, and the darkest areas, associated with the "holes" in the Re atom layer between the metal clusters. In the valence band images (e.g., Figure 7), the Se(3) and Se(4) atom positions are brighter than the Se(2) and Se(1) positions although they are farther away from the tip by 0.34 Å. Consequently, atoms closer to the tip do not necessarily dominate tunneling images.

In conclusion we would like to emphasize the need for an interplay between theory and experiment in the analysis of atomic resolution STM and AFM images. Layered transition metal dichalcogenide surfaces are relatively simple since they have no dangling bonds or surface reconstructions. Nevertheless, we found it challenging to deconvolute the topological and electronic contributions to the STM and AFM images of the surface of $ReSe_2$.

(11) The single bias images are taken at higher resolution (400 × 400 pixels) and can be scanned more quickly.

Experimental Section

The STM and AFM used in this study was a Nanoscope II from Digital Instruments, Santa Barbara, CA, which aquires images of 400 × 400 pixels. Electrochemically etched tungsten or platinum tips were used for STM, the preparation of which is described in ref 1g. Micromachined polycrystalline silicon cantilevers, as supplied by the AFM manufacturer, were used for the AFM measurements. Crystals of unintentionally doped $ReSe_2$ were prepared by a chemical vapor transport procedure similar to that described in ref 8 and had n-type conductivity. The thin plate-like crystals were mounted with Ag epoxy onto Cu disks and were cleaved with sticky tape prior to each STM or AFM experiment. Details of the STM and AFM conditions are given in the figure captions.

Acknowledgment. Work at North Carolina State University is supported by the U.S. Department of Energy, Office of Basic Energy Sciences, Division of Materials Sciences, under Grant DE-FG05-86ER45259. We thank Scott McLean for help in crystal growing and Ed Delawski for assistance in the AFM images.

Registry No. $ReSe_2$, 12038-64-1.

An Experimentally Based Family of Potential Energy Surfaces for Hydride Transfer between NAD^+ Analogues[1]

Yongho Kim, Donald G. Truhlar, and Maurice M. Kreevoy*

Contribution from the Chemical Dynamics Laboratory. Department of Chemistry. University of Minnesota. 207 Pleasant St., S.E., Minneapolis. Minnesota 55455. *Received November 13, 1990*

Abstract: A family of three-body potential energy surfaces has been constructed to model experimental rate constants, k_r, for hydride transfer between NAD^+ analogues in a 2-propanol–water solvent at 25 °C. The potential energy surfaces are analytical expressions for potential energy as functions of atom and group coordinates. They permit the use of variational transition-state theory (VTST) and large-curvature semiclassical tunneling approximations to calculate reaction rates. In previous work, about 50 experimental rate constants, k_{ij}, spanning a range of 10^{11} in equilibrium constant, K_{ij}, and 10^6 in k_{ij}, were fitted to a simplified form of Marcus theory which we now call linearized Marcus theory. With the aid of this formalism and four parameters, all rate constants for hydride transfer under the specified conditions can be reproduced. The average discrepancy between calculated and observed rate constants is a factor of 1.6. Primary kinetic isotope effects (KIEs) were also measured, for a range of K_{ij}. Structure variation in the donor leads to an increase in the KIE when K_{ij} is increased, while structure variation in the acceptor leads to a decrease in the KIE when K_{ij} is increased, both in accord with linearized Marcus theory. The rate constants and KIEs calculated by the VTST-plus-tunneling method were also treated by linearized Marcus theory. The parameters of the potential energy surface were varied to optimize the agreement between computational and experimental isotope effects, and the same four Marcus parameters for both hydride and deuteride transfer. All the relevant qualitative features of the experimental results were reproduced, and the quantitative agreement is satisfactory. The C–H stretching frequencies of the reactants and products are also reproduced. The most probable critical configurations in the VTST-plus-tunneling calculations involve tunneling at heavy-atom separations greater than that of the transition state (corner-cutting tunneling). About 1 kcal mol^{-1} of the barrier is evaded by tunneling. Tunneling has a major effect on the calculated KIE values and their variation with K_{ij}, and it has a perceptible effect on the Marcus parameters. Because so many characteristics of the experimental k_{ij} values are reproduced, we conclude that the potential functions are a reasonable representation of the real potential energy functions governing the hydrogenic motions, at least in the neighborhood of reactants and critical configurations.

1. Introduction

The theory of reaction rates has evolved from two quite different points of view, which may be called the phenomenological and the model based approaches. In the former, correlations of rate constants with the corresponding equilibrium constants are identified, and primary and secondary kinetic isotope effects and sometimes the activation parameters are determined. Then the formalism and concepts of transition-state theory[2] are used to attribute various qualitative features to the transition states. However, while trends can be predicted, little quantitative information about activated structures has been available from this approach. As a result, it is often hard to be sure that the magnitude of a suggested effect is consistent with the suggested ex-

(1) This work is supported, in part, by the U. S. National Science Foundation, through Grant Nos. CHE 89-00103 and CHE 89-922048, and, in part, by a grant for computing time by the Minnesota Supercomputer Institute.

(2) Kreevoy, M. M.; Truhlar, D. G. In *Rates and Mechanisms of Reactions*: Bernasconi, C. F., Ed.; Wiley: New York, 1986; Chapter 1.

0002-7863/91/1513-7837$02.50/0

planation. It is also hard to be confident that the various suggested characteristics of a transition state are mutually consistent. In one version of the modeling approach, potential energy surfaces have been fitted to semiempirical or ab initio quantum mechanical electronic structure calculations, and transition-state theory has been used to calculate reaction rates. However, the generation of potential energy surfaces is so time consuming that only the simplest systems can be studied in this way.[3] Even the prediction of barrier heights is still beyond the state of the art for most reactions. The generation of more complete potential energy surfaces, required by variational transition-state theory, is much more difficult still. It has been very difficult to use the modeling approach to mimic the wealth of results which have been produced for inherently complicated reactions, occurring in solution.

In the present paper the first approach is pursued in conjunction with the second approach, and in this way some of the faults and difficulties of both approaches are alleviated. A family of global potential energy surfaces which permits us to mimic a large and diverse body of experimental results for hydride transfer between nicotinamide adenine dinucleotide (NAD^+) analogues is described. Our potential energy surfaces are analytic functions of three internal coordinates, corresponding to three-body models $(A_i\text{–}H\text{–}A_j)^+$ of the reactive systems, where A_i^+ and A_j^+ are NAD^+ analogues. A_i^+ and A_j^+ are represented in the potential functions by two "extended atoms", called C_1 and C_2, which have masses of 15 daltons. The potential functions are intended to mimic the effects of additional degrees of freedom of the solute and also reactant–solvent interactions. We believe that they provide the best available description of events near the critical configurations.

In an earlier paper[4] a family of empirically modified extended LEPS[5] potentials were used to show that the hydrogen transfers considered here are dominated by tunneling. The critical configurations[6,7] were found to be far from the conventional transition states (the saddle points on the potential energy surfaces[2]). In particular, they were found to have considerably larger $C_1\text{–}C_2$ separations than the transition states.[4] Although the Born–Oppenheimer approximation[8] was assumed to be satisfied so that the potential energy functions and saddle points were exactly the same for hydrogen and deuterium variants of the system, the most probable $C_1\text{–}C_2$ separations were greater for hydride tunneling than for deuteride tunneling.

This led to the prediction of a number of experimental results, all of which have now been reported[4,9] either for hydride transfer or proton transfer, or both. However, the potential energy surfaces, which were intended to model hydride transfer between NAD^+ analogues in solution, failed to reproduce several aspects of the experimental results. While rate constants calculated from these potential energy surfaces could be fitted to the Marcus theory of atom transfer,[2,10] as can experimental hydride transfer rate constants,[11] the work term, W^r, required to fit the calculated rate constants was much larger than that required by the experimental values, which is around zero.[11,12] Further the calculated primary kinetic isotope effect (KIE) was around 20 when the equilibrium constant, K_{ij}, was 1.0.[4] The calculated KIE values also showed a sharp maximum at that K_{ij} when the acceptor C–H bond strength was varied to produce a range of K_{ij} values.[4] The experimental KIE, on the other hand, has not been observed to exceed 6.[4,9,13] Further the experimental KIE increases with K_{ij} for substituents in the hydride donor[9] but decreases as K_{ij} increases for substituents in the hydride acceptor.[4] The experimental results were easily accommodated within phenomenological Marcus theory, but they were not mimicked by the results calculated from the model potentials.[4]

Both in the earlier work[4] and the present work, improved canonical variational transition-state theory[14] with large curvature ground-state tunneling was used to calculate rate constants. These rate constants were fitted to Marcus theory just as if they were experimental rate constants. The resulting Marcus parameters and isotope effects were compared with the experimental values, and the parameters of the potential function were adjusted to improve the match. In the present work the potential energy surfaces were readjusted, and the calculation of Marcus parameters and KIEs was repeated until an optimal match was achieved between the parameters based on calculation and those based on experiments. In this way we have obtained a family of three-body potential energy surfaces which successfully approximate the behavior of all Marcus theory parameters (W^r, λ, τ), the values of the KIE, trends in KIE with K_{ij}, as well as the bond dissociation energies and vibration frequencies.

The starting point for the new potential energy surfaces, as before, is a family of extended LEPS potential.[5] We then add terms representing the interactions of charges in a dielectric medium[15] and an adjustable barrier widening function,[4,16] which is used to bring the calculated isotope effects into reasonable agreement with experimental results.

2. Marcus Theory

Marcus theory was originally derived for outer-sphere electron transfer.[17] It was extended by analogy to atom and group transfer.[2,10,11,18–21] It has not been derived from any molecular model of atom or group transfer, nor is there any clearly implied model. However, two considerations make the Marcus formalism a very useful and easily applied framework for relating rate constants, k_r, to equilibrium constants, K_{eq}. First, it equates $\ln k_r$ to the first few terms of a power series in $\ln K_{eq}$.[2] (The number of terms retained in the series depends on the variant of the theory used.[2]) If only the first-order term is retained, it becomes the Brønsted catalysis law.[22] This "law" is already sufficient for representing a large amount of data. A formalism that adds higher order terms to it should be even more broadly applicable, and, indeed, many types of theoretical[23] and experimental[2,20,24] rate constants have been successfully fitted to the Marcus formalism. Second, it suggests an interpretation for the coefficients.[2,11,18] In the present work we investigate whether the Marcus formalism

(3) Truhlar, D. G.; Steckler, R.; Gordon, M. S. *Chem. Rev.* **1987**, *87*, 217.
(4) Kreevoy, M. M.; Ostović, D.; Truhlar, D. G.; Garrett, B. C. *J. Phys. Chem.* **1987**, *90*, 3766.
(5) Kuntz, P. J.; Nemeth, E. M.; Polanyi, J. C.; Rosner, S. D.; Young, C. E. *J. Chem. Phys.* **1966**, *44*, 1168.
(6) "There is ... always some intermediate configuration which is critical for the process, in the sense that if this system is attained, there is a high probability that the reaction will continue to completion." Glasstone, S.; Laidler, K. J.; Eyring, H. *The Theory of Rate Processes*; McGraw Hill: New York, 1941; p 10.
(7) The critical configuration has been defined as the most probable structure for crossing the hardest-to-attain dividing surface that separates reactants from products.[4]
(8) Born, M.; Oppenheimer, J. R. *Ann. Phys.* **1927**, *84*, 457.
(9) Kreevoy, M. M.; Lee, I.-S. H. *Z. Naturforsch.* **1989**, *44a*, 418.
(10) Marcus, R. A. *J. Phys. Chem.* **1968**, *72*, 891.
(11) Kreevoy, M. M.; Ostović, D.; Lee, I.-S. H.; Binder, D. A.; King, G. *J. Am. Chem. Soc.* **1988**, *110*, 524.
(12) Lee, I.-S. H.; Ostović, D.; Kreevoy, M. M. *J. Am. Chem. Soc.* **1988**, *110*, 3989.
(13) Ostović, D.; Roberts, R. M. G.; Kreevoy, M. M. *J. Am. Chem. Soc.* **1983**, *105*, 7629.
(14) (a) Truhlar, D. G.; Isaacson, A. D.; Garrett, B. C. In *Theory of Chemical Reaction Dynamics*; Baer, M., Ed.; CRC Press: Boca Raton, FL, 1985; Vol. 4, p 65. (b) Garrett, B. C.; Truhlar, D. G.; Wagner, A. F.; Dunning, T. W. *J. Chem. Phys.* **1983**, *78*, 4400. (c) Garrett, B. C.; Abusalbi, N.; Kouri, D. J.; Truhlar, D. G. *J. Chem. Phys.* **1985**, *83*, 2252. (d) Garrett, B. C.; Joseph, T.; Truong, T. N.; Truhlar, D. G. *Chem. Phys.* **1989**, *136*, 271. (e) Truhlar, D. G.; Garrett, B. C. *J. Chim. Phys.* **1987**, *84*, 365.
(15) (a) Hoijting, G. J.; de Boer, E.; van der Meij, P. H.; Weijland, W. P. *Recl. Trav. Chim. Pays-Bas*, 1956, *75*, 487. (b) Chalvet, O.; Jano, I. *C. R. Seances Acad. Sci.* **1965**, *261*, 103. (c) Kozaki, T.; Morihashi, K.; Kikuchi, O. *J. Am. Chem. Soc.* **1989**, *111*, 1547. (d) Tucker, S. C.; Truhlar, D. G. *Chem. Phys. Lett.* **1989**, *57*, 164.
(16) Truhlar, D. G.; Horowitz, C. J. *J. Chem. Phys.* **1978**, *68*, 2466.
(17) Marcus, R. A. *J. Chem. Phys.* **1956**, *24*, 966.
(18) Kreevoy, M. M.; Lee, I.-S. H. *J. Am. Chem. Soc.* **1984**, *106*, 2550.
(19) Roberts, R. M. G.; Ostović, D.; Kreevoy, M. M. *Faraday Discuss. Chem. Soc.* **1982**, *74*, 257.
(20) Albery, W. J.; Kreevoy, M. M. *Adv. Phys. Org. Chem.* **1978**, *16*, 87.
(21) Lewis, E. S.; Hu, D. D. *J. Am. Chem. Soc.* **1984**, *106*, 3292.
(22) (a) Brønsted, J. N.; Pederson, J. J. *Z. Phys. Chem.* **1924**, *108*, 185. (b) Brønsted, J. N. *Chem. Rev.* **1928**, *5*, 322.
(23) (a) Murdoch, J. R. *Faraday Discuss. Chem. Soc.* **1982**, *74*, 297. (b) Donnella, J.; Murdoch, J. R. *J. Am. Chem. Soc.* **1984**, *106*, 4724. (c) Wolfe, S.; Mitchell, D. J.; Schlegel, H. B. *J. Am. Chem. Soc.* **1981**, *103*, 7694.
(24) Albery, W. J. *Annu. Rev. Phys. Chem.* **1980**, *31*, 227.

can be used to correlate k_r values calculated from three-body models for the reacting systems, we use such calculations to inquire into the physical significance of the Marcus theory parameters, and we identify the particular parameters of the potential energy surfaces that have the most influence on each of the Marcus parameters.

In the Marcus theory of atom or group transfer, the reactive event is visualized in three stages: first, reactant conversion to precursor configuration, a process that has a standard Gibbs free energy of W^r; second, precursor configuration conversion through the transition state (or other critical configuration[6,7]) to a successor configuration, a process that has a standard Gibbs free energy of $\Delta G^{\circ\prime}$ and a standard Gibbs free energy of activation of $\Delta G^{\ddagger}$; and, finally, the conversion of the successor configuration to products, a process that has a standard Gibbs free energy of $-W^p$. In reactions of the type under consideration here, W^r is thought to arise from the negative entropy of bringing the reactants together and properly aligning them, from a positive desolvation enthalpy, and from the negative enthalpy of charge transfer interaction between the reactants.[11] It is thought to be approximately independent of the structural details of the reactants and to be near zero.

We apply the Marcus formalism to the reaction shown in eq 1.

$$A_i^+ + A_jH \rightarrow A_iH + A_j^+ \quad (1)$$

The equilibrium constant is given in eq 2 and the transition-state theory rate constant is given in eq 3.

$$K_{ij} = \exp(-\Delta G^{\circ}/RT) \quad (2)$$

$$k_{ij} = (k_BT/h)\exp(-\Delta G^{*}/RT) \quad (3)$$

The free energy of activation for the second step, $\Delta G^{\ddagger}$, is given in terms of the free energy change of this step and an intrinsic barrier, $\lambda/4$, for this step by eq 4.

$$\Delta G^{\ddagger} = \lambda/4 + \Delta G^{\circ\prime}/2 + \Delta G^{\circ\prime 2}/4\lambda \quad (4)$$

Equation 5 relates the standard Gibbs free energy of the overall reaction, ΔG°, to that for the second step, $\Delta G^{\circ\prime}$.[2]

$$\Delta G^{\circ\prime} = \Delta G^{\circ} - W^r + W^p \quad (5)$$

If A_i^+ and A_j^+ are structurally similar, W^r and W^p are assumed to be equal, and, in that case, which applies in this paper, $\Delta G^{\circ\prime}$ is equal to ΔG°. Equation 6 gives the overall reaction standard Gibbs free energy of activation, ΔG^{*}, as a sum of $\Delta G^{\ddagger}$ and W^r.

$$\Delta G^{*} = \Delta G^{\ddagger} + W^r \quad (6)$$

$\Delta G^{\ddagger}$ is strongly structure-sensitive, and W^r is not. Equation 7 relates λ to the corresponding parameters for two symmetrical reactions of the same type as that shown in eq 1.[2]

$$\lambda = (\lambda_{ii} + \lambda_{jj})/2 \quad (7)$$

We note that eq 4, which is the heart of Marcus theory, requires a quadratic relation between a set of activation energies, $\Delta G^{\ddagger}$, and the standard free energies, $\Delta G^{\circ\prime}$, for the same set of reaction steps.

In the Marcus theory, the energy required to distort the nuclei of the precursor configuration into the geometry of the successor configuration, without the accompanying covalency change, is λ.[2] It is called the reorganization energy. For a symmetrical variant of the reaction ($K_{ij} = 1$), attainment of the transition state requires half the distortion required to attain the successor configuration. It therefore requires one-fourth of the energy, $\lambda/4$, since the harmonic approximation is made.[2] This quantity, $\lambda/4$, is known as the intrinsic barrier. For the symmetrical reactions related to the reactants and products of eq 1, the intrinsic barriers are called $\lambda_{ii}/4$ and $\lambda_{jj}/4$, respectively.

For a series of structurally similar symmetrical hydride transfer reactions, λ_{ii} should be a function of the tightness parameter, τ,[20] and the standard free energy for the transfer of hydride from a standard donor,[25] $A_j{}^{\circ}H$, to A_i^+.[18,21] The standard free energy of transfer is $\Delta G_{ij}^{\circ\circ}$. To infer the nature of the function and to suggest a formal definition of τ, a number of idealized cases have been considered.[18] In the first set of idealized cases it is postulated that the critical configurations for symmetrical hydride transfer are triple ions, $A_i^+H^-A_i^+$. In that case all A_i–H bond energy is lost in forming the critical configuration, and if $\Delta G_{ij}^{\circ\circ}$ becomes more negative, ΔG_{ii}^{*} becomes more positive by an equal amount. Since W^r is constant, $\lambda_{ii}/4$ increases by the same amount as ΔG_{ii}^{*}. Recalling eq 2 and 3, $[\delta(\ln k_{ii})/\delta(\ln K_{ij}^{\circ})]_{W^r,j}$ is minus one. In the second set of idealized cases it is postulated that the two A_i–H bonds in the symmetrical critical configurations have combined energy equal to the A_i–H bond energy in the reactants. In that case ΔG_{ii}^{*}, $\lambda_{ii}/4$, and k_{ii} are all independent of $\Delta G_{ij}^{\circ\circ}$ and $[\delta(\ln k_{ii})/\delta(\ln K_{ij}^{\circ})]_{W^r,j}$ is zero. In the third set of idealized cases, each of the two A_i–H bonds in the critical configurations have the same bond energies that they have in the reactants. That is, the total A_i–H bond energy in each critical configuration is twice the A_i–H bond energy in the reactants from which it was formed. In that case, if $\Delta G_{ij}^{\circ\circ}$ becomes more negative, ΔG_{ii}^{*} and $\lambda_{ii}/4$ also becomes more negative, by an equal amount, and $[\delta(\ln k_{ii})/\delta(\ln K_{ij}^{\circ})]_{W^r,j}$ is one. These idealized cases led to the definition of τ by eq 8,[18] which gives the three values the thought experiments require and is consistent with an earlier, qualitative definition.[20]

$$\tau - 1 = [\delta(\ln k_{ii})/\delta(\ln K_{ij}^{\circ})]_{W^r,j} \quad (8)$$

They also led to the idea that τ could be identified with the sum of the bond orders to the in-flight hydrogen.[4,18] That idea will be shown in this paper to be quantitatively inaccurate, although trends in τ values do parallel trends in the sum of bond orders to the in-flight atom. For this reason τ is called the tightness parameter.

The other partner in the general reaction, A_j^+ (eq 1) can be treated in the same way. When these two results are combined, using eq 7, eq 9 is obtained.

$$[d\lambda/d(\Delta G^{\circ})]_{W^r} = 2(\tau - 1) \quad (9)$$

Instead of experimentally determining λ_{ii} and λ_{jj} for each unsymmetrical reaction, a linearized version of Marcus theory has been used,[2,11,18] in which the τ value was assumed to be constant. This yields

$$\lambda = \lambda_0 + [\delta\lambda/\delta(\Delta G^{\circ})]_{W^r}\Delta G^{\circ} \quad (10)$$

where λ_0 is λ for the special case where both K_{ij}° (the equilibriium constant for the standard reaction discussed above) are unity. Equations 4, 6, and 10 have been successfully applied to a large body of experimental rate constants for hydride transfer between NAD^+ analogues.[11]

In summary, the four parameters of linearized Marcus theory are λ, τ, W^r, and W^p. Since A_i^+ and A_j^+ are structurally similar in the present study, we assume $W^r = W^p$ so there are only three independent parameters. We now proceed to develop a family of potential energy surfaces from which k_{ij} values can be calculated which will be in accord with the experimental values for the three parameters and with the experimental results for the isotopic variation of these parameters.

3. The Potential Function

The assumed potential energy surface for the collinear, three-body model of the reaction shown in eq 1 is given in eq 11.

$$V = V_{ELEPS} + V_W + V_{CD} + V_{solv} \quad (11)$$

V_{ELEPS} is an extended LEPS function[5] and V_W is a widening function.[16] Taken together, V_{CD} and V_{solv} are intended to mimic, in a rudimentary way, the interaction of charges with each other, with another polarizable reactant, and with the solvent. Since the surfaces are adjusted to fit rate constants obtained in solution and include free energy of solvation, they represent potentials of mean force. The extended LEPS potential function is given in eq 12–16.

(25) For practical and historic reasons 10-methylacridan has been used as A_jH, and the required equilibrium constants have been measured.[11,18]

$$V_{ELEPS} = \frac{Q_{ab}}{1+k_{ab}} + \frac{Q_{bc}}{1+k_{bc}} + \frac{Q_{ac}}{1+k_{ac}} - \left[\frac{1}{2}\left\{\left(\frac{J_{ab}}{1+k_{ab}} - \frac{J_{bc}}{1+k_{bc}}\right)^2 + \left(\frac{J_{bc}}{1+k_{bc}} - \frac{J_{ac}}{1+k_{ac}}\right)^2 + \left(\frac{J_{ab}}{1+k_{ab}} - \frac{J_{ac}}{1+k_{ac}}\right)^2\right\}\right]^{1/2} \quad (12)$$

$$E^1_{ab} = D_e(ab)[e^{-2\beta_{ab}|r_{ab}-r_e(ab)|} - 2e^{-\beta_{ab}|r_{ab}-r_e(ab)|}] \quad (13)$$

$$E^3_{ab} = \tfrac{1}{2}D_e(ab)[e^{-2\beta_{ab}|r_{ab}-r_e(ab)|} + 2e^{-\beta_{ab}|r_{ab}-r_e(ab)|}] \quad (14)$$

$$E^1_{ab} = (Q_{ab} + J_{ab})/(1 + k_{ab}) \quad (15)$$

$$E^3_{ab} = (Q_{ab} - J_{ab})/(1 - k_{ab}) \quad (16)$$

Q_{ab} is a Coulomb integral, J_{ab} is an exchange integral, E^1_{ab} is the potential energy for singlet bonded a and b, E^3_{ab} is the repulsive potential for triplet antibonding a and b, and β_{ab}'s are Morse range parameters. The k_{ab}'s are Sato parameters and were given the values 0.55 for C–H interactions and 0.20 for C–C interactions. Equilibrium dissociation energies are $D_e(ab)$'s, and $r_e(ab)$'s are equilibrium bond lengths.

As a reference reactant, we have used a reactant with a C–H dissociation energy, $D_e°(CH)$, of 73 kcal mol^{-1}, an equilibrium C–H distance, $r_e°(CH)$, of 1.118 Å, and a range parameter, $\beta_{o,CH}$, of 2.175 Å^{-1}. These dissociation energies[26a] and bond lengths[26b] are approximately those for a doubly allylic hydrogen, and the dissociation energies are similar to those that have been measured or deduced for analogous structures.[27] Using standard formulas,[28] these reference values generate a harmonic C–H stretching frequency of 2937 cm^{-1}. Other reactants were generated by changing $D_e(CH)$ in the range 58–83 kcal mol^{-1}. The bond energy bond order method (BEBO),[29] eq 17, was then used to maintain consistent values of $r_e(CH)$.

$$r_e(CH) = r_e°(CH) - 0.5\text{Å} \log\left(\frac{D_e(CH)}{D_e°(CH)}\right) \quad (17)$$

The coefficient of the logarithmic term in eq 17 was given the value 0.5 Å, somewhat smaller than the value commonly used for C–C bonds.[29] This value was deduced by Johnston[30] from the activation energy of the reaction of CH_3 with H_2. Presumably it is smaller than the corresponding value for C–C bonds because of the relative insensitivity of C–H bond length[26a] to change in bond energy.[26b] A constant harmonic C–H stretching force constant was maintained as the bond dissociation energy was changed by applying eq 18 to the β values.

$$\beta = \beta_o\sqrt{D_e°(CH)/D_e(CH)} \quad (18)$$

The singlet and triplet energies, E^1 and E^3, of the reactant and product C–H bonds are obtained, in eq 13 and 14, from quantities which were adjusted to reproduce the geometric and spectroscopic properties of the reactants. If the two carbon atoms of the real reactants were brought into bonding distance, their interaction would be similar to the interplanar C–C interaction in graphite, because of the structures in which they are incorporated in the NAD^+ analogues under consideration here. We have, therefore, based the initial choices of β, r_e and r for the C–C "bond" on the interplanar properties of graphite,[31] and final adjustments were made to reproduce the experimental Marcus parameters. This yields $D_e(CC)$ = 8.07 kcal mol^{-1}, $r_e(CC)$ = 3.228 Å, and β_{CC} = 1.890 Å^{-1}. The Q's and J's were adjusted by solving eq 15 and 16. The C–H Sato parameters had to be made relatively large to avoid large, positive values of W^r. Although it is not obvious from the above equations, the Sato parameters scale the pairwise antibonding atomic interactions. If the C–H repulsion is allowed to be large, it makes a major contribution to ΔG^*, and, since the magnitude of this contribution is not related to $\Delta G°'$, a large, positive value of W^r is obtained. Such values of W^r have been observed in proton transfers,[32] but the reaction we are modeling here requires a W^r near zero.[11] To get a near-zero value for W^r, k_{CH} was given a value of 0.55. The other Sato parameter, k_{CC}, also plays a major role in determining ΔG^*. It was given a value of 0.20 to bring the calculated ΔG^* into approximate agreement with the experimental results.[11]

The LEPS surface is known to give a too narrow barrier for the well-studied H + H_2 reaction.[33] When an unmodified LEPS surface was used, the calculated kinetic isotope effect was too large, so it was first modified by adding terms of the form[16] shown in eq 19 to widen the barrier.

$$V_a = a[(r_{C_1H} - r_{C_2H})(r_{C_1H} - r_{CC}) \times (r_{C_2H} - r_{CC})]^n \exp[-\alpha(r_{C_1H} + r_{C_2H} + r_{CC})^3] \quad (19)$$

The three internuclear distances were labeled r_{C_1H}, r_{C_2H}, and r_{CC}. But we could not reproduce the experimental Marcus parameters with this widening function.[4] This function has a value of zero when the two bond lengths are equal, and in the reactant and product structures. But for the unsymmetrical reactions, the two bond lengths are not equal at the saddle point. We believe that the use of the V_a function in our previous work[4] contributed to the calculated free energy of activation in a way that made the calculated W^r much too large. To solve this problem in the present study, we have now introduced the widening function shown in eq 20, which goes to zero at the saddle point and is close to zero everywhere on the transition state dividing surface between reactants and products.

$$V_W = A_W\frac{(r^*_{C_1H}r_{C_2H} - r^*_{C_2H}r_{C_1H})^2}{(r^*_{C_1H} + r^*_{C_2H})^2}(r^*_{C_1H}r_{C_2H} + r^*_{C_2H}r_{C_1H})^2 \exp\left\{-\beta_W\left(\frac{r^*_{C_1H}r_{C_1H} + r^*_{C_2H}r_{C_2H}}{r^*_{C_1H} + r^*_{C_2H}}\right)^4\right\} \quad (20)$$

For each reaction, the r^* values in eq 20 are equated to the C–H distance at the saddle point in a preliminary calculation without the widening function. They are, therefore, not exactly the C–H distances at the saddle points for the final surfaces, but the differences are only on the order of 10^{-6} Å. The A_W and β_W parameters were then adjusted to give reasonable values to the kinetic hydrogen isotope effect and the Marcus W^r. Good agreement with experimental results was obtained using values A_W = 83.1 kcal mol^{-1} Å^{-6} and β_W = 0.47 Å^{-4}. Since W^r is also sensitive to other parameters of the potential energy surfaces, notably the Sato parameters of the LEPS surface, other combinations of parameters which will reproduce the experimental results probably exist. However, we believe that such combinations would give similar values of V at the critical geometries. The exponential term in eq 20 causes V_W to die off when either C–H distance is large. The preexponential term makes the widening function zero at the saddle point even though the reaction is not symmetric. The r^*'s in the exponential term were used to reduce the widening function selectively on the high-energy side of the dividing surface. We use variational transition-state theory with semiclassical transmission coefficients[14,34] to calculate rate constants. For the series

(26) (a) Gordon, A. J.; Ford, R. A. In *The Chemist's Companion: A Handbook of Practical Data, Techniques, and References*; John Wiley: New York, 1972; p 107. (b) Reference 26a, p 113.
(27) Stein, S. E.; Brown, R. L. *J. Am. Chem. Soc.* **1991**, *113*, 787.
(28) Herzberg, G. In *Molecular Spectra and Molecular Structure. I. Spectra of Diatomic Molecules*; D. Van Nostrand: New York, 1950; pp 101–102.
(29) (a) Pauling, L. *J. Am. Chem. Soc.* **1947**, *69*, 542. (b) Johnston, H. S.; Parr, C. *J. Am. Chem. Soc.* **1963**, *85*, 2544.
(30) Johnston, H. S. *Adv. Chem. Phys.* **1960**, *3*, 131.
(31) Kelly, B. T. In *Physics of Graphite*; Applied Science Publishers: London, 1981; pp 50–85.
(32) Kreevoy, M. M.; Oh, S.-W. *J. Am. Chem. Soc.* **1973**, *95*, 4805.
(33) Truhlar, D. G.; Wyatt, R. E. *Adv. Chem. Phys.* **1977**, *36*, 141.
(34) Garrett, B. C.; Truhlar, D. G.; Grev, R. S.; Magnuson, A. W. *J. Phys. Chem.* **1980**, *84*, 1730.

of surfaces studied here, the variational transition state tends to be located on the high-energy side of the saddle point. As the variational transition state moves away from the saddle point, it is raised by the widening function. Without the $r^{\ddagger}$'s in the exponential term of the widening function, the variational transition state energy would increase too rapidly with increasing $\Delta G°$, resulting in too high a value of W^{T}.

In the hydride transfer reaction between NAD^+ analogues, the donor is a polarizable molecule and the acceptor has a positive charge, so a charge-induced dipole term, as formulated in eq 21, has been included.

$$V_{CD} = -A_{CD}[(C/r_{CC})^4 - (C/r_{CC})^8] \quad (21a)$$

$$A_{CD} = 95.381 \text{ kcal mol}^{-1} \quad (21b)$$

$$C = 2.421 \text{ Å} \quad (21c)$$

This can also, to some extent, play the role of the unknown charge-dipole term with empirical adjustment of parameters. A short-range repulsion term is also included in eq 21, to reduce the effect of the charge-induced dipole term on the overall free energy of activation, which we preferred to model by adjusting the parameters of the LEPS function. The parameter C serves to locate the charge-induced dipole energy minimum, and it has a significant effect on W^{T}. It was adjusted to keep W^{T} approximately the same for endothermic and exothermic reactions. It gives a minimum values of V_{CD} at $r_{CC} = 2.879$ Å.

Solvent molecules are usually assumed to be equilibrated with the internal charge distribution of the reacting substances.[35a] In the present case the contribution of solvation energy to V was estimated using a generalized Born formula[15]

$$V_{solv} = -\frac{1}{2}\left(1 - \frac{1}{\epsilon}\right)\sum_a \frac{q_a^2}{r_a} - \frac{1}{2}\left(1 - \frac{1}{\epsilon}\right)\sum_a \sum_{b \neq a} \frac{q_a q_b}{r_{ab}} \quad (22)$$

The dielectric constant of the solvent, which we set arbitrarily at 40, is ϵ; a and b are any two of C_1, H, and C_2; r_{ab} is the distance between a and b; r_{C_1}, r_H, and r_{C_2} are the van der Waals radii; and q_a is the fractional charge of atom or group a. It is known that the Born formula overestimates the free energy of hydration of ions when the bulk value for the dielectric constant and the crystallographic radii of the ions are used.[36] However, Rashin and Honig have shown that the original Born model gives reasonable results for monatomic ions if appropriate radii are used.[37] Therefore, we decided to use van der Waals radii for the Born formula. In particular, we used 2.0 Å for C_1 and C_2 and 1.2 Å for H.[26b]

The atomic charges at the critical configurations are obtained as follows. In the Marcus theory of atom and group transfer, τ represents the tightness of the critical configuration.[18,20] The charge of the in-flight H at the critical configurations is modeled by $\tau - 1$.[18] The experimental τ value for the hydride transfer reaction we are trying to mimic is about 0.80,[11] so the charge of the in-flight hydride at the symmetrical critical configurations, for which $r_{C_1H} = r_{C_2H}$, was given the value −0.2. We represented the charges as functions of the distances between carbons and the hydride in flight by eq 23–25.

$$q_{C_1} = 3/\{3 + 2\exp(r_{C_2H} - r_{C_1H})\} \quad (23)$$

$$q_{C_2} = 3/\{3 + 2\exp(r_{C_1H} - r_{C_2H})\} \quad (24)$$

$$q_H = 1 - (q_{C_1} + q_{C_2}) \quad (25)$$

The values of q_{C_1}, q_{C_2}, and q_H in terms of $r_{C_2H} - r_{C_1H}$, for the symmetric reaction, are shown in Figure 1.

We note that, because the generalized Born solvation energy does not vanish in the reactant and product regions, the actual

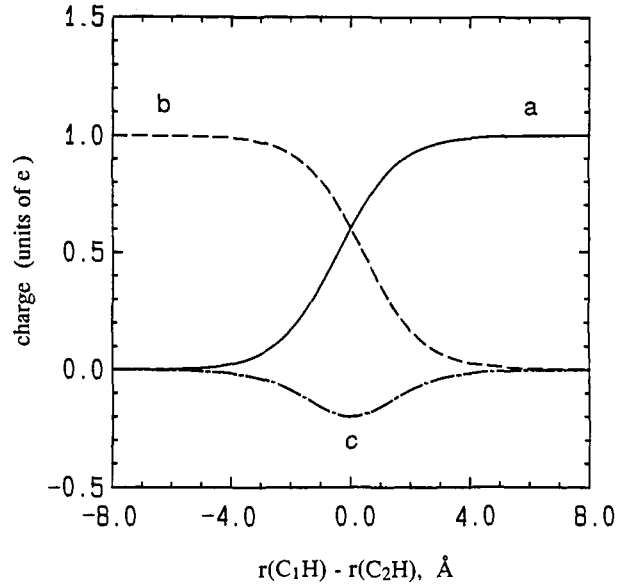

Figure 1. The charges on the acceptor carbon (a), the donor carbon (b), and the hydrogen (c) as function of the difference between the two C–H distances, for collinear configurations, according to eq 23–25.

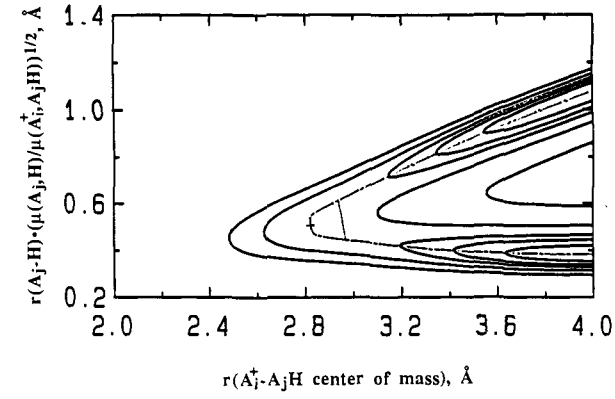

Figure 2. Potential energy contours, minimum energy path (dot–dash line) and tunneling path connecting classical turning points at the most probable tunneling energy at 300 K (light solid line) for a collinear, three-body model of hydride transfer from A_jH to A_i^+. A_i and A_j represent two atoms, C_1 and C_2, which have mass of 15 daltons; $r(A_i–A_jH)$ is the distance from the center of mass of the A_jH moiety to the third body A_i and $r(A_j–H)$ is the distance between A_j and H. Reactant and product bond strengths are both 73 kcal mol^{-1}. Orthogonal, mass-scaled coordinates are used. The zero of energy is defined as the bottom of the reactant vibrational well. The saddle point is shown at +. The most probable reaction path involves tunneling. The representative tunneling path shown is explained at the end of section 4.

energy changes for the processes $A_iH \rightarrow A_i^+ + H^-$ and $A_jH \rightarrow A_j^+ + H^-$ are not given simply by the D_e values in the extended LEPS term. Nevertheless, because of the way the charges are defined in eq 23–25, the reactant vibrational frequency may still be obtained simply from the Morse parameters. These parameters have been adjusted to give frequencies in agreement with experiment, as described above. The shape of the potential energy surface near the saddle point and critical configurations, including the Born solvation term, has been adjusted to reproduce the experimental kinetic results.

The resulting potential energy surface for hydride transfer is shown in Figure 2, in mass-scaled, orthogonal coordinates.[35b,38] The potential energy surface is shown in coordinates scaled for the deuteride transfer in Figure 3. The skew angle[14] for hydride transfer is small, 20°, so tunneling in configurations more extended

(35) (a) Reference 6, pp 401–403. (b) *Ibid.*, pp 100–107. (c) *Ibid.*, pp 85–86, 184–185.
(36) Latimer, W. M.; Pitzer, K. S.; Slansky, C. M. *J. Chem. Phys.* **1939**, *7*, 108.
(37) Rashin, A. A.; Honig, B. *J. Phys. Chem.* **1985**, *89*, 5588.
(38) (a) Levine, R. D.; Bernstein, R. D. In *Molecular Reaction Dynamics and Chemical Reactivity*; Oxford University Press: New York, 1987; p 165. (b) Garrett, B. C.; Truhlar, D. G. *J. Phys. Chem.* **1979**, *83*, 1052.

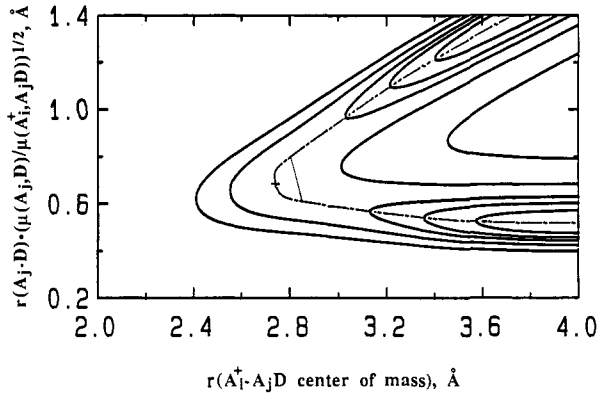

Figure 3. The same as Figure 2, except for deuteride transfer.

than the saddle point (conventional transition state) is quite significant. For deuteride transfer the skew angle increases to 28°. This reduces the tunneling probability, particularly in more extended configurations, and shifts the most probable point of barrier penetration to a less extended configuration, closer to the saddle point. It is interesting to compare the potential energy surface of Figure 2 to the one used in our previous study.[4] In that case the saddle point geometry and barrier height for the reference symmetric reaction were characterized by $r^{\ddagger}_{C_1H}$ = 1.36 Å and $V^{\ddagger}$ = 21.1 kcal mol^{-1}, whereas the present potential energy surface has $r^{\ddagger}_{C_1H}$ = 1.46 Å and $V^{\ddagger}$ = 18.3 kcal mol^{-1}. The previous saddle point vibrational frequencies were 442 cm^{-1} for the stretch, 639 cm^{-1} for the bend, and 1758i cm^{-1} for the reaction coordinate, whereas the present values for these frequencies are 622, 836, and 997i cm^{-1}, respectively. We see from these frequencies that the new bound modes are tighter, and the barriers are flatter near the saddle points and the critical configurations.

The variation of the four terms contributing to V (eq 11) as a hydride system passes along the minimum energy path from reactants to products (see Figure 4). The justification for V will lie in the many aspects of the experimental results that it permits us to reproduce.

4. Calculation of Rate Constants

The rate constants for the three-body models were calculated by improved canonical variational transition-state theory (ICVT)[14,34] with the large curvature ground-state (LCG3) tunneling approximation[14] using the program POLYRATE.[39,40] We identify the A_i^+ and A_j^+ of section 2 with C_1 and C_2 of section 3; the masses of A_i^+ and A_j^+ were set equal to 15 daltons in all cases. In carrying out the ICVT and LCG3 calculation, the three-body potential of mean force of section 2 was treated as an ordinary potential energy. Rotational and vibrational partition functions are approximated by the independent mode approximation, with rigid rotations and harmonic vibrations.[14a] All calculations reported in this paper are for a temperature of 300 K.

The bimolecular rate constant including tunneling is given[14a] by the expression

$$k_{ij} = k(\mathrm{ICVT})\kappa(\mathrm{LCG3}) \qquad (26)$$

where the "quasi-classical rate constant" k(ICVT) corresponds to classical reaction coordinate motion with other degrees of freedom quantized. Variational transition-state theory selects the transition states from species lying on the minimum potential energy path from reactants to products by maximizing the quasi-thermodynamic free energy of activation.[41] (In contrast

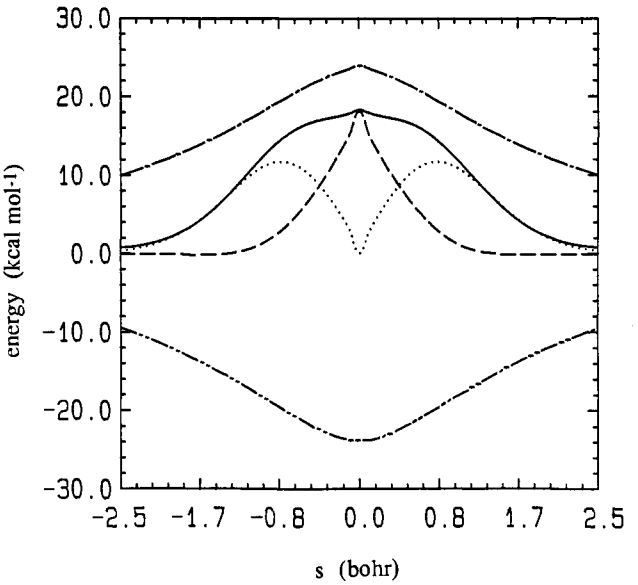

Figure 4. Calculated total energy, and its constituents, along the minimum energy path, for a hydride transfer with reactant and product bond strengths both 73 kcal mol^{-1}. The LEPS function is --- (eq 12). The widening function is ··· (eq 20). Ion-induced dipole interaction is –··– (eq 21). The generalized Born energy is –·– (eq 22). The total is —. The mass-scaled reaction coordinate, s, is the distance from the saddle point, measured along the minimum energy path, in the coordinate system shown in Figure 2. Positive values of s indicate progress toward products; negative values, reversion toward reactants.

conventional transition-state theory locates the transition state at the point on the minimum energy path which maximizes the potential energy.[2])

In the present case, for the symmetric reaction with C–H bond energy of 73 kcal mol^{-1}, the potential energy maximum on the minimum energy path is symmetrical, with C–H bond lengths of 1.46 Å. However, because the zero-point energy rises rapidly on either side of the symmetric structure, two equivalent free energy maxima exist, symmetrically displaced from the potential energy maximum. One of these has a donor C–H bond length of 1.34 Å and an acceptor of 1.60 Å. In the other, the donor and the acceptor bond lengths are reversed. Between them there is a shallow local free energy minimum, whose maximum depth is 0.47 kcal mol^{-1}. In order to mimic experimental results for unsymmetrical reactions, the bond dissociation energy of A_i–H was changed systematically to generate exo- or endothermic reactions. For symmetrical reactions both the A_i–H and A_j–H bond strengths were changed simultaneously. For exoergic reactions the earlier maximum serves as the overall transition state, but for endoergic reactions the later maximum is the overall transition state. Once the transition state has been located, variational transition-state calculations are made in the same way as conventional transition-state calculations.[14,34,39-41]

The quasi-classical kinetic isotope effect, KIE_{qc}, is k_H(ICVT)/k_D(ICVT). It is determined principally by changes in zero-point energy and rotational partition functions.

The transmission coefficient κ(LCG3) accounts in principle for all quantum effects on the reaction coordinate, although tunneling is the most important.[13,34,41] In the formalism employed here,[14,34] the transmission coefficient is always calculated for ground-state reactants in the exoergic direction. It involves a thermal average over total energy, E:

$$\kappa(\mathrm{LCG3}) = \frac{1}{k_BT}\exp\left(\frac{V_a^{AG}}{k_BT}\right)\int_{\epsilon^{RG}}^{\infty} P^G(E)\exp\left(-\frac{E}{k_BT}\right)dE \qquad (27)$$

where V_a^{AG} is the vibrationally adiabatic ground-state energy at the zero-temperature variational transition state, ϵ^{RG} is the zero-point energy of reactant, and $P^G(E)$ is the ground-state tunneling probability calculated by the LCG3 algorithm for estimating corner-cutting tunneling effects semiclassically. The

(39) Isaacson, A. D.; Truhlar, D. G.; Rai, S. N.; Steckler, R.: Hancok, G. C.; Garrett, B. C.; Redmon, M. J. *Comput. Phys. Commun.* **1987**, *47*, 91.
(40) Lu. D.-H.; Truong, T. N.; Melissas, V. S.; Garrett, B. C.; Steckler, R.; Isaacson, A. D.; Rai, S. N.; Hancock, G. C.; Lauderdale. J. G.; Joseph, T.; Truhlar, D. G. POLYRATE, Version 3.0; University of Minnesota: Minneapolis, unpublished.
(41) (a) Garrett, B. C.; Truhlar, D. G. *J. Chem. Phys.* **1979**, *70*, 1593. (b) Tucker, S. C.; Truhlar, D. G. In *New Theoretical Concepts for Understanding Organic Reactions*; Bertran, J., Csizmadia, I. G., Eds.; Kluwer Academic Publishers: Boston, 1989; pp 291–346.

tunneling contribution to the kinetic isotope effect is κ_H(LCG3)/κ_D(LCG3). The tunneling probability in eq 27 should be summed over all the vibrational states of the exoergic products that are significantly populated. In the present case, however, we included only ground-state-to-ground-state tunneling. In additional calculations not reported here in detail, we tested this approximation by recalculating the rate constants for the isoenergetic reaction and the most exoergic of the reactions reported in Table IV. Including tunneling into excited product states by the methods used previously,[4,14c] again with harmonic vibrations, caused a 3% increase in k_{ij}(H) in the exoergic case and an 0.3% increase in the isoenergetic case. These changes would tend to reduce W^r by less than 1 kcal mol^{-1}, and they do not change our results significantly.

Since tunneling into excited states of the product was much more important in our previous study,[4] it is of considerable interest to comment on the potential energy surface difference that primarily changes the conclusion about the role of vibrationally assisted tunneling (VAT). The principal feature that decreases VAT on the new surface is that both the potential energy V and the vibrationally adiabatic ground-state potential[34] decrease much less rapidly after the saddle point is passed. Consider, for example, the case with $D_e(A_j\text{–H})$ = 73 kcal mol^{-1} and $D_e(A_i\text{–H})$ = 83 kcal mol^{-1}. On both the old and new surface the saddle point is early for this case, with $r_{A_iH} > r_{A_jH}$ by 0.1–0.2 Å. If we proceed to the point where r_{A_jH} increases 0.4 Å beyond its value at the saddle point, we find on the old surface that V drops from 17.7 to 7.2 kcal mol^{-1} and V_a^G drops 7.8 kcal mol^{-1}. Vibrationally excited states can already be accessed with positive kinetic energies at this location. On the new surface, though, V drops only from 13.7 to 13.0 kcal mol^{-1}, and V_a^G has decreased to only 0.15 kcal mol^{-1} below its value at the saddle point. Tunneling into an excited state would require a tunneling path ending with r_{A_jH} extended almost 0.5 Å further out into the product valley, and such a long tunneling path has a very small tunneling probability associated with it.

For the potential energy function used here, the minimum energy path (MEP) has the transferred H atom lying on a straight line from the acceptor, A_i, to the donor, A_j. For such a collinear MEP, the dominant tunneling paths of the LCG3 approximation are collinear. For discussion purposes in the next section we will identify a representative tunneling path, a representative pretunneling configuration, and a representative critical configuration. These all refer to a temperature of 300 K, and they are defined as follows. First we find the energy, E_{rep}, at which the integrand, $P^G(E)\exp(-E/k_BT)$, of eq 27 is a maximum. This is called the representative or most probable tunneling energy. (For example, for the symmetrical reaction with D_e = 73 kcal mol^{-1}, E_{rep} = 21.3 kcal mol^{-1}, which is 0.7 kcal mol^{-1} below V_a^{AG}.) At this energy the tunneling path with the smallest A_i–A_j distance is taken as representative; examples of such representative tunneling paths in the semiclassical LCG3 approximation,[14b-d] are shown in Figures 2 and 3. Along such a path, the system proceeds with positive kinetic energy along the minimum energy path until the vibrationally adiabatic ground-state potential energy curve V_a^G equals E_{rep}; then it tunnels along a straight line through the mass-scaled coordinate system to the point in the product valley where V_a^G again equals E_{rep}. The representative pretunneling configuration is identified with the point in the reactant valley where $V_a^G = E_{rep}$, and the representative critical configuration is identified with the point of highest potential energy along the straight-line tunneling path. In general, analyzing the full range of reactions studied here, both symmetrical and unsymmetrical, with D_e(CH) = 58–83 kcal mol^{-1}, the representative critical configurations for hydride transfer have C–C distances 0.138–0.147 Å greater than the saddle point value. The representative critical configurations for deuteride transfer have critical configurations 0.088–0.099 Å greater than the corresponding saddle point values.

5. Results and Discussion

The calculated rate constants, transmission coefficients, and kinetic isotope effects for symmetrical reactions are shown in Table I. Linearized Marcus theory, eq 8–10, predicts that a plot of

Table I. Calculated Rate Constants, Transmission Coefficients, and KIEs for Symmetrical Reactions[a]

D_e(CH)[b]	k_{ii}(H)[c]	KIE$_{qc}$	κ(H)	κ(D)	KIE
83.0	8.43×10^{-4}	1.89	2.27	1.21	3.71
80.5	1.27×10^{-3}	1.88	2.79	1.28	4.09
78.0	2.11×10^{-3}	1.86	3.56	1.36	4.86
75.5	3.00×10^{-3}	1.82	3.82	1.45	4.80
73.0	5.67×10^{-3}	1.78	5.32	1.54	6.16
70.5	7.88×10^{-3}	1.79	5.30	1.64	5.80
68.0	1.53×10^{-2}	1.85	7.22	1.85	7.21
65.5	2.32×10^{-2}	1.92	7.39	2.02	7.00
63.0	4.60×10^{-2}	1.99	9.67	2.27	8.48
60.5	1.02×10^{-1}	2.09	13.7	2.60	11.0
58.0	1.65×10^{-1}	2.21	13.6	2.91	10.3

[a] At 300 K. [b] The bond dissociation energies for donors and acceptors in kcal mol^{-1}. [c] M^{-1} s^{-1}.

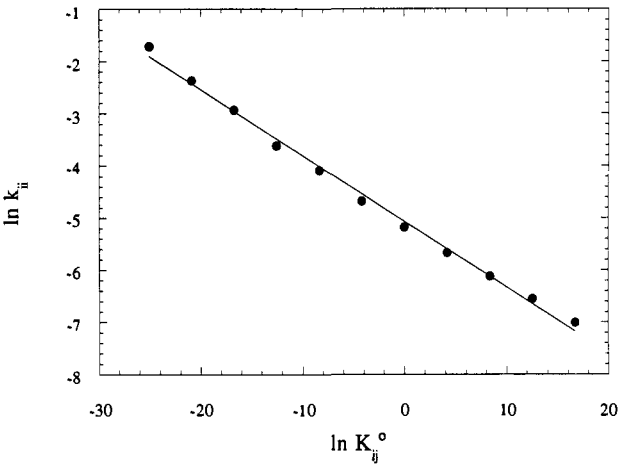

Figure 5. The variation of rate constants for symmetrical reactions, k_{ii}, with changes in the equilibrium constant for unsymmetrical reactions transferring a hydride to A_i^+ from a standard donor with a bond strength of 73 kcal mol^{-1}. $K_{ij}°$ and k_{ii} were made to vary by changing C–H bond strengths as described in the text. This plot is assumed to be linear in linearized Marcus theory, and its slope is $\tau - 1$. Actually, some curvature is apparent, in the sense that the slope becomes less negative (τ becomes larger) as the A_i–H bond becomes stronger. The curvature is not strong, however, and a linear relation, namely, ln k_{ii} = −5.150 − 0.126 ln $K_{ij}°$, represents the relation with an average absolute value of the discrepancy of ~8% in k_{ii}. This relation is parallel to a tangent to the curve at ln $K_{ij}°$ = −5. It gives a value of 0.874 for τ_H.

ln k_{ii} against ln $K_{ij}°$ should be linear with a slope of $\tau - 1$ (eq 10). The $K_{ij}°$'s in eq 8 are the equilibrium constants for transfer of hydride from a standard donor, HA_j, to a series of acceptors, A_i^+, of varying C–H bond strength; the k_{ii}'s are rate constants for the symmetric reactions in which the bond strength of both the donor and acceptor are changed to the new value. Such a plot is shown in Figure 5. Because computational results have little scatter, and because a large range of $K_{ij}°$ values was spanned, the points in Figure 5 can be seen to define a curved line. However, the curvature is slight. The best linear relation between ln k_{ij} and ln $K_{ij}°$, fitted by the method of least squares, is shown in Figure 5. The average discrepancy between the computed k_{ii} values and those corresponding to the least-squares line in Figure 5 is 8%. A similar departure from linearity would not be detectable in the experimental results.[11] The best linear relation between ln k_{ii} and ln $K_{ij}°$ has a slope of −0.13, leading to a value of 0.87 for τ_H, which may be compared with the best experimental value, 0.80.[11] The limited number of experimental points and their scatter preclude a test for the curvature which is shown by the calculated points.

The comparable plot for deuteride transfer is shown in Figure 6. It has a similar shape, but, at any given value of $K_{ij}°$, it has a slightly larger slope. The least-squares line covering the same range of ln $K_{ij}°$ values has a slope of −0.10, which leads to a τ_D value of 0.90. As expected from the interpretation of τ as a tightness parameter and the shorter C–C distance found in the representative critical configurations for deuteride transfer (nu-

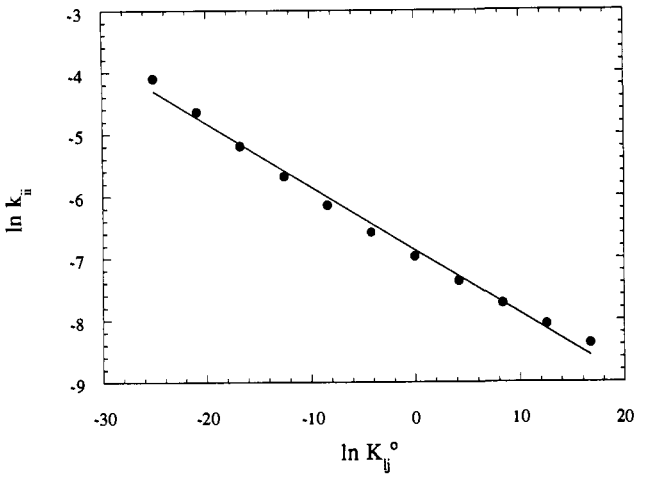

Figure 6. The same as Figure 5, except for deuteride transfer. The best linear relation through the points in this case is $\ln k_{ii} = -6.885 - 0.101 \ln K_{ij}°$. Thus τ_D is 0.899 and $\tau_D - \tau_H$ is 0.025.

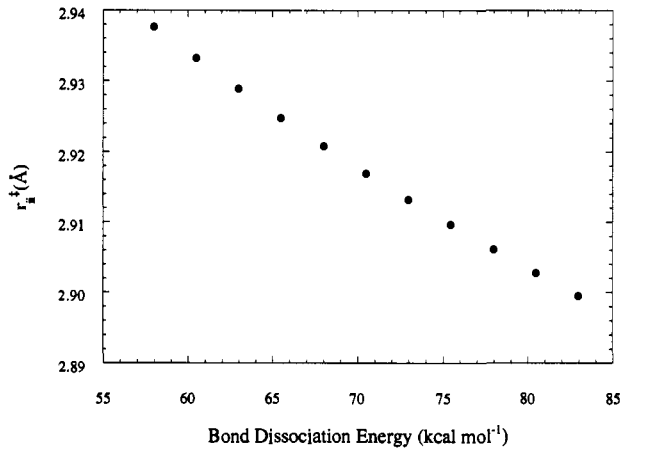

Figure 7. The A_i–A_j separation at the saddle point for symmetric reactions. The bond dissociation energies in the acceptor and the donor are varied. The A_i–A_j separation at the variational transition state is very similar and varies in the same way with bond dissociation energies.

merical values are given above and examples are shown in Figures 2 and 3), τ_D is a little larger than τ_H, even though hydride and deuteride transfer are governed by the same potential energy surface. There is no experimental value with which τ_D can be directly compared, but the difference between τ_H and τ_D gives rise to a characteristic pattern of variations in the KIE with ln $K_{ij}°$, which is described below and compared with experiment.

The curvature seen in Figures 5 and 6 implies that τ becomes progressively smaller as the reactant and product C–H bonds become weaker. The quantitative discrepancy between the experimental τ value of 0.80 and the value of 0.87 obtained from the model could be reduced by making the calculations for smaller C–H bond energies. However, in practice, a bond energy of 33 kcal mol^{-1} would be required. This is an unreasonable value, and it would lead to very unrealistically large isotope effects. The discrepancy between computational and experimental τ values is due either to oversimplifications in the model, errors in the potential function, or experimental errors. However, the two τ values are similar enough for our present purposes.

As shown in Figure 7, as the product and reactant C–H bonds are made weaker, and τ becomes smaller, the saddle point C–C distance increases. The C–C distance at the most probable critical configuration behaves similarly. Thus, τ correlates with the geometric expansion or contraction of the critical configuration, as well as with the strength of its partial bonds. However, τ does not appear to be numerically equal to the sum of the bond orders at the in-flight hydrogen, as was originally suggested.[18] Table II shows the bond orders, n, calculated for the most probable

Table II. Bond Orders in Activated Configurations

configuration	$n(C_1–H)$	$n(C_2–H)$	n(total)
saddle point	0.210	0.210	0.420
critical configuration	0.154	0.154	0.380
pretunneling configuration	0.051	0.466	0.517

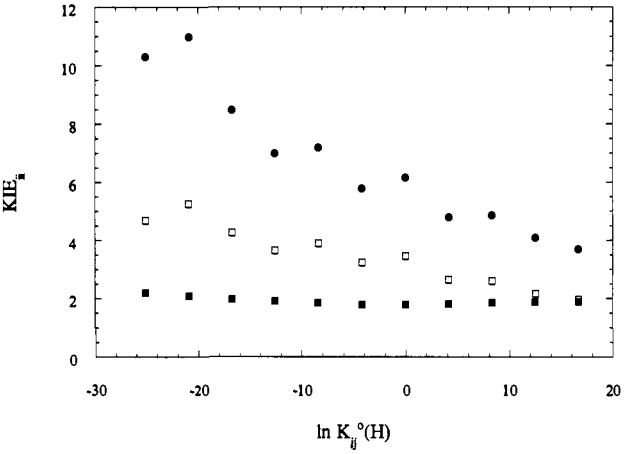

Figure 8. Isotope effects on symmetric reactions as a function of $K_{ij}°$ for unsymmetrical transfer of hydride from a standard donor, with bond dissociation energy of 73 kcal mol^{-1}. The symmetric reactions were varied by simultaneously changing the donor and the acceptor bond strengths, and the unsymmetrical reactions were varied by changing only the acceptor bond strength. The filled circles are the overall KIEs, the open squares are the tunneling contributions to the overall KIEs, and the filled squares are the quasi-classical contributions to the overall KIEs.

critical configuration, for the case with product and reactant C–H bond energy of 73 kcal mol^{-1}. The most probable or representative critical configuration was defined, above, as the configuration of the highest classical potential energy at the most probable tunneling energy at 300 K. The bond orders were calculated from reactant bond lengths by means of eq 28.[29,30]

$$r = r_e - (0.5\ \text{Å}) \log n \qquad (28)$$

Table II also shows the bond orders at the saddle point (conventional transition state) and at the classical turning point at the most probable tunneling energy. The sums of the calculated bond orders are about half of τ. Thus, τ appears to have the qualitative, but not the quantitative significance that was ascribed to it.[18,20]

Figure 8 shows the calculated quasi-classical and tunneling contributions to the kinetic isotope effects and the overall KIE for symmetrical reactions, as a function of the bond energy of the donor and acceptor C–H bonds. The quasi-classical contribution to the KIE is almost constant, but the tunneling contribution to the KIE and, consequently, the total KIE increase significantly as the C–H bond energy decreases. For hydride transfer reactions with $1.0 < K_{ij} < 10^2$, carried out in hydroxylic solvents, KIE values generally lie between 5.0 and 5.5,[13,42] although for one system a value of 6.0 has been obtained.[43] (The use of nonhydroxylic solvents gives rise to lower KIE values,[42,43] but also leads to dynamic complexities which are outside the scope of this paper.) The total calculated KIE for energetically symmetrical hydride transfers becomes 6.2, which is close to the range of measured values when the C–H bond energy is 73 kcal mol^{-1}. At this point the calculated quasi-classical contribution to the KIE is 1.8, and the tunneling contribution to the KIE is 3.5. The experimental KIE has been interpreted in terms of quasi-classical and tunneling components by studying its solvent dependence.[42,43] An experimental upper limit to the quasi-classical factor, obtained in this way, is ~2.6, and the corresponding lower limit to the tunneling

(42) Kreevoy, M. M.; Kotchevar, A. T. *J. Am. Chem. Soc.* **1990**, *112*, 3579.
(43) Kreevoy, M. M.; Kotchevar, A. T. *J. Phys. Chem.*, accepted for publication.

Table III. The Effect of the Equilibrium C–C Distance on the KIE for Symmetrical Reactions

$R_e(CC)^a$	$r^*(CC)^a$	$\nu^*(H)^b$	$\Delta V_a^{AG}(H)^c$	$KIE_{qc}{}^d$	$k(H)^e$	$\kappa(H)/\kappa(D)$	KIE
3.228	2.90	989	17.83	1.78	5.65×10^{-3}	3.46	6.16
3.254	2.93	1118	19.04	2.31	1.34×10^{-3}	3.99	9.22
3.281	2.95	1234	20.22	3.47	2.90×10^{-4}	3.73	12.92
3.307	2.97	1342	21.60	3.92	5.71×10^{-5}	6.74	26.42

[a] In units of Å. [b] The imaginary frequency at the saddle point in units of cm^{-1}. [c] The maximum of the vibrationally adiabatic ground-state potential energy curve in units of kcal mol^{-1}, relative to the zero-point energy level of the reactants. [d] KIE_{qc} is obtained by dividing the overall KIE by $\kappa(H)/\kappa(D)$. [e] In units of M^{-1} s^{-1}.

factor is ~2.0.[42] Considering the uncertainties in the interpretation of the experimental values and the sensitivity of the calculated result to the shape of the barrier, we consider this agreement between the experimental values and the values given by the molecular model very encouraging.

The tunneling contribution to the KIE increases, in symmetrical reactions, as the C–H bond becomes weaker, because such reactions have larger C–C distances in the neighborhood of the saddle point. The effect of the C–C separation on the KIE is also shown by increasing $r_e(CC)$ while holding all other potential parameters constant for the symmetrical reaction with D_e = 73 kcal mol^{-1}. These results are given in Table III. This table shows the C–C bond distance, $r^*(CC)$, and imaginary frequency at the saddle point, the vibrationally adiabatic ground-state barrier height, and some of the results of the dynamic calculations, all as functions of $r_e(CC)$. The table shows that both the quasi-classical and the tunneling contributions to the KIE approximately double with an 0.08-Å increase in the equilibrium C–C distance. The origin of the increase in the quasi-classical KIE is complicated, because the variational transition state shifts as the C–C distance is increased, and the shift in the deuterium-containing transition state is not completely synchronous with the shift in the hydrogen-containing transition state. However, this does not affect the tunneling contribution to the KIE, as the tunneling does not take place at the transition state in any event. The tunneling isotope effect becomes larger as the equilibrium C–C distance increases because more energy is required to reach the transition state, as shown in Table III, and tunneling then becomes energetically more profitable. Without changing any other parameter of the potential function, increasing the equilibrium C–C distance also increases the imaginary frequency at the saddle point, and this also tends to promote tunneling.

Increasing the equilibrium C–C distance is equivalent to introducing bulky substituents to impede the close approach of the reactants. This has long been known to increase kinetic isotope effects.[44,45] From its discovery this effect was thought to be associated with tunneling, but it was thought that a "narrower"[46] barrier would have to be produced by the bulky substituents. In our earlier paper[4] we pointed out that corner-cutting tunneling would produce an increase in the tunneling contribution to the KIE when the approach of the reactants was hindered, without requiring any special shape of the potential energy surface. Since then, detailed calculation by Wolfe and co-workers has tended to confirm this.[47] The present paper further strengthens the suggestion that corner-cutting tunneling is an important factor in the steric exaltation of isotope effects. This conclusion is traceable to large-curvature tunneling,[14,34,41] and does not require any special modification of the potential energy surface.

The calculated equilibrium constants, rate constants, transmission coefficients, and kinetic isotope effects for unsymmetrical reactions are shown in Table IV.

Figure 9 is a Brønsted plot with structure variation in the acceptor. It shows that the $k_{ij}(H)$'s give an acceptable Brønsted correlation,[22] although slight curvature is visible. (Because of experimental scatter and molecular idiosyncrasy, such curvature would be hard to detect using experimental results.) The least-squares slope, α, is 0.46. Equation 29 gives the linearized Marcus theory expression for the Brønsted α, with χ defined by eq 30.[18,21]

$$\alpha = \chi + 0.5(\tau - 1) - 0.5(RT \ln K_{ij}/\lambda)^2(\tau - 1) \quad (29)$$

$$\chi = 0.5[1 - (RT/\lambda) \ln K_{ij}] \quad (30)$$

The least-squares straight lines given by both the Brønsted plot (Figure 9) and the plot of ln k_{ii} against ln K_{ij}° (Figure 5) are actually tangents to the curves defined by the points at about ln K_{ij} = −4 or ln K_{ij}° = −4. The λ value appropriate to such a value of ln K_{ij} or ln K_{ij}° is ~83 kcal mol^{-1}, so χ is 0.50. Equation 29 then gives 0.44 for α, in excellent agreement with the least-squares slope obtained from Figure 9. There is no directly comparable experimental result, but, since linearized Marcus theory generally fits the experimental results,[11] and the experimental τ is 0.80, an

Table IV. Calculated Equilibrium Constants, Transmission Coefficients, Rate Constants, and KIEs for Unsymmetrical Reactions[a]

$D_e(A_iH)^b$	K_{ij}	$k_{ij}(H)^c$	$k_{ji}(H)^c$	$\kappa(H)$	$\kappa(D)$	KIE_{ij}
83.0	1.8×10^{7}	5.62	3.07×10^{-7}	2.88	1.29	4.27
80.5	2.8×10^{5}	1.05	3.74×10^{-6}	3.42	1.40	4.64
78.0	4.3×10^{3}	1.77×10^{-1}	4.14×10^{-5}	3.75	1.46	4.76
75.5	6.6×10	3.23×10^{-2}	4.94×10^{-4}	4.52	1.53	5.37
73.0	1.0	5.67×10^{-3}	5.67×10^{-3}	5.32	1.54	6.16
70.5	1.5×10^{-2}	7.36×10^{-4}	4.81×10^{-2}	4.93	1.63	5.38
68.0	2.4×10^{-4}	1.15×10^{-4}	4.92×10^{-1}	5.67	1.70	5.94
65.5	3.6×10^{-6}	1.67×10^{-5}	4.66	6.24	1.80	6.23
63.0	5.5×10^{-8}	2.31×10^{-6}	4.22×10	6.77	1.89	6.48
60.5	8.4×10^{-10}	2.55×10^{-7}	3.04×10^{2}	6.04	1.99	5.56
58.0	1.3×10^{-11}	2.78×10^{-8}	2.16×10^{3}	5.53	2.04	5.02

[a] At 300 K. [b] The bond dissociation energies for acceptors in kcal mol^{-1}. The bond dissociation energy of donors is fixed at 73 kcal mol^{-1}. [For the $k_{ji}(H)$ column, these are the bond dissociation energies for the donors, and the standard value is used for the acceptor.] [c] $k_{ij}(H)$ and $k_{ji}(H)$ are forward and reverse rate constants, respectively, in units of M^{-1} s^{-1}.

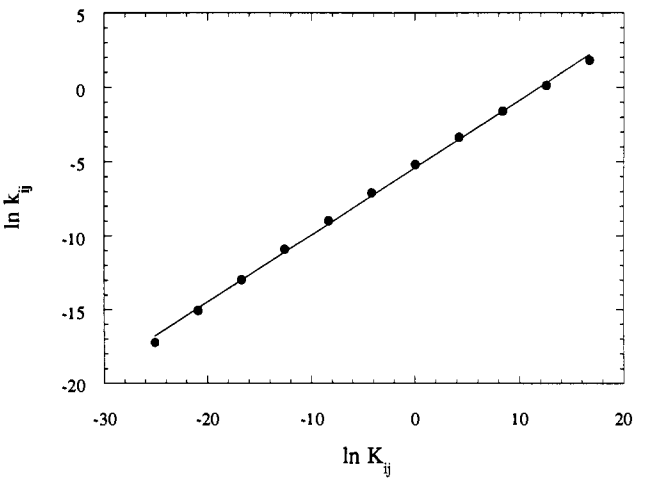

Figure 9. A Brønsted plot of computed rate constants. In the absence of experimental error and molecular idiosyncrasy, slight curvature is visible. The least squares representation of the results is: ln k_{ij} = −5.476 − 0.457 ln K_{ij}.

(44) Lewis, E. S.; Funderburk, L. H. *J. Am. Chem. Soc.* **1967**, *89*, 2322.
(45) Melander, L.; Saunders, W. H., Jr. In *Reaction Rates of Isotopic Molecules*; John Wiley: New York, 1980; p 152.
(46) The width of the energy barrier for a bimolecular reaction is not well defined. We believe that the intent of the original authors[41] was to suggest that the bulky substituents increased the imaginary frequency at the saddle point.
(47) Wolfe, S.; Hoz, S.; Kim, C.-K.; Yang, K. *J. Am. Chem. Soc.* **1990**, *112*, 4186.

experimental α of 0.40 can be expected. Taken all together these results give strong support to the quantitative formulation of τ.[18,21]

To proceed further in our analysis of the results, we need a value for W^τ. (W^p does not enter into the equations because it is assumed to equal W^τ; thus it cancels out in eq 5 but W^τ is still needed in eq 6.) For simplicity, and because it is consistent with the experimental results,[11,12] the potential energy surface was adjusted until the results were consistent with $W^\tau = 0$. In our earlier work[4] a value of 18.5 kcal mol^{-1} was obtained for W^τ, and, at an intermediate stage of the present work, intermediate values of W^τ were obtained. As indicated above, it has been conventionally thought that W^τ represents the standard free energy of formation of a precursor configuration from the reactants.[2,10,11,17] However, there are no local energy or free energy minima corresponding to any of these values of W^τ, and it does not appear that W^τ is the standard free energy of formation of any well-defined structure from the reactants. It appears to have only the significance given to it by eq 6. It is a free energy which is subtracted from ΔG^*, chosen so that the rest, $\Delta G^\ddagger$, may be calculated using eq 4, with the additional constraint that W^τ should be independent of K_{ij} or nearly so.

Using eq 3 and 4, with $W^\tau = 0$, each of the k_{ii} in Table I gives a λ_{ii} (or λ_{ii}) value. For unsymmetrical reactions, λ can then be calculated from eq 7. The value of λ_{jj} for the standard donor is found to be 82.6 kcal mol^{-1}, and the values of λ_{ii} for the various acceptors are in the range 78.5–84.8 kcal mol^{-1}. The Marcus theory k_{ij}'s were calculated from eq 3, 4, and 7 (still using $W^\tau = 0$). The average discrepancy between Marcus theory values of k_{ij}(H) and those given in Table IV is 0.3%. Alternatively λ_{ii} (or λ_{jj}) values can be obtained from the linearized Marcus theory expression, eq 9 and 10. These values turn out to be in a similar range, namely, λ_{ii} = 78.7–85.0 kcal mol^{-1}, and they were used, as above, to calculate linearized Marcus theory values of k_{ij}. On average, these differ too from the values in Table IV by only 0.3%. Thus both the original Marcus formalism and the linearized version give excellent correlations of the calculated ICVT/LCG3 rate constants, just as they do for measured ones. Linearized Marcus theory, with the definition of τ which is imbedded in it, gives an excellent approximation of the original theory.

W^τ = −2 kcal mol^{-1} was used in treating the experimental results.[11] For values between 2 and −2 kcal mol^{-1}, the choice of W^τ has very little impact on the correspondence between Marcus theory calculation and the experimental results. Furthermore, the values we obtained for λ_{ii} are in good agreement with the experimental[11] values, which are in the range 85–98 kcal mol^{-1}; these values would be 83–96 kcal mol^{-1} if $W^\tau = 0$ had been used in treating the experimental results. This, combined with the satisfactory agreement mentioned above for the τ_H and the similar values of W^τ used with the experimental and computed results, indicates that we have achieved the goal set forth at the end of section 2.

We now consider the isotopic dependence of the Marcus parameter τ. Because τ_H and τ_D are different (Figures 5 and 6), the linearized Marcus formalism and the original Marcus formalism both make the superficially unexpected prediction that changing K_{ij} will not have the same effect on the KIE when the acceptor is changed as it does when the donor is changed.[4,9] This occurs because, to get $K_{ij} > 1.0$ by changing the acceptor, the acceptor C–H bond must be made *stronger* than the standard C–H bond, and the isotope effect on k_{ii} is reduced (Figure 8). This leads to a reduced isotope effect on λ_{ii}, and when the λ_{ii} for H and D are recombined with the standard λ_{jj} for H and D, we get a *reduced* isotope effect on λ. This, in turn, leads to a *reduced* KIE. On the other hand, if it is the donor which is changed to get $K_{ji} > 1.0$, then the donor C–H bond must be made *weaker* than the standard. The same process outlined above then gives an *increased* isotope effect on λ. If the change in ΔG° is not too large, an *increased* KIE is predicted. In the absence of tunneling, $\tau_D - \tau_H$ is very small; it is 0.004 using variational transition-state theory and 0.002 using conventional transition-state theory. Furthermore, including tunneling only along the minimum energy path, gives much smaller transmission coefficients than the LCG3 method. (For example, for the symmetrical reaction with D_e = 73 kcal mol^{-1} minimum-energy-path tunneling[14a] gives κ_H = 1.11 and κ_D = 1.04, as compared to LCG3 values of κ_H = 5.32 and κ_D = 1.54.) Thus corner-cutting tunneling is responsible for the dependence of kinetic isotope effect on K_{ij}.[4,9] We do not believe that any molecular model which reproduces the other aspects of the experimental results will give $\tau_D - \tau_H$ of the required magnitude without corner-cutting tunneling. The effect of $\tau_D - \tau_H$ on the KIE is quantified in eq 31 (substitution in the donor) and 32 (substitution in the acceptor),[9] and the results are shown in Figure 10.

$$\ln (KIE) = \ln (KIE^\circ) + 0.5 \ln K_{ij} (\tau_H - \tau_D) - 0.5RT(\ln K_{ij})^2(1/\lambda_H - 1/\lambda_D) \quad (31)$$

$$\ln (KIE) = \ln (KIE^\circ) - 0.5 \ln K_{ij}(\tau_H - \tau_D) + 0.5RT(\ln K_{ij})^2(1/\lambda_H - \lambda_D) \quad (32)$$

Experimentally, such a result has already been demonstrated for hydride transfer.[9] It is shown in Figure 11. The correspondence

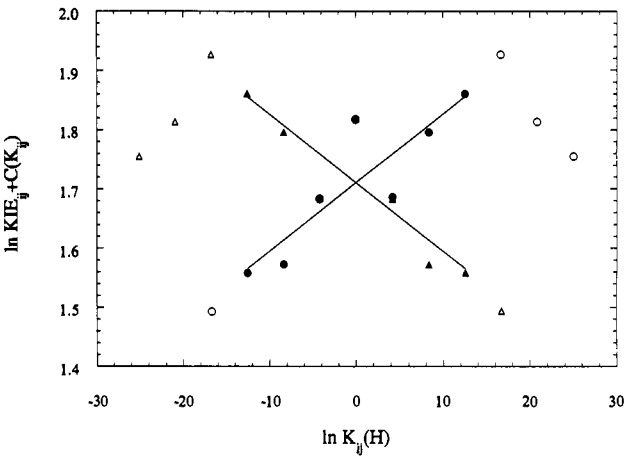

Figure 10. The variation of the computed ln KIE$_{ij}$ + $C(K_{ij})$ with ln K_{ij}, plotted as suggested by linearized Marcus theory. $C(K_{ij}) = -0.5RT(\ln K_{ij})^2(1/\lambda_H - 1/\lambda_D)$. Triangles represent the result of bond strength variation in the acceptor; circles, the results of bond strength variation in the donor. The lines are the least-squares lines through the filled points and represent the relation which exists close to the origin. The slopes of the lines are ±0.0116, and they yield a value of 0.0232 for $\tau_D - \tau_H$.

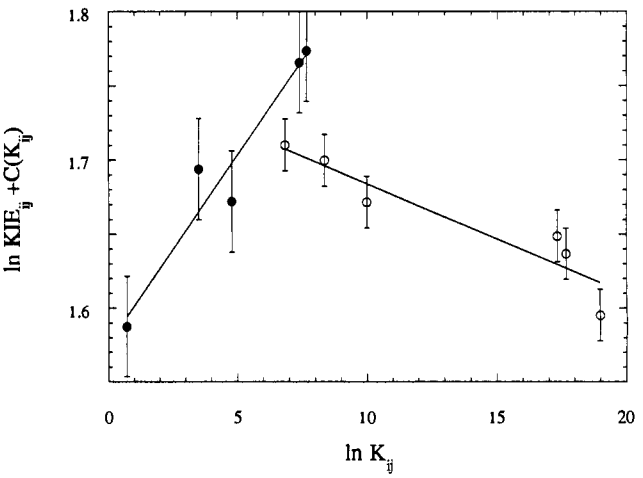

Figure 11. The variation of experimental ln KIE$_{ij}$ + $C(K_{ij})$ plotted as suggested by linearized Marcus theory, in the same way that the computed results are plotted in Figure 10. $C(K_{ij}) = 0.5RT(\ln K_{ij})^2(1/\lambda_H - 1/\lambda_D)$. Filled points are for structure variation in the donor; open points for structure variation in the acceptor. (One of the points was misplotted in the original publication.) Estimated probable errors are shown. The least-squares lines, shown, have slopes of 0.025 and −0.0075, leading to values of 0.050 and 0.015 for $\tau_D - \tau_H$. These may be compared with the value, 0.024, obtained from computed KIE values (Figure 10).

between Figures 10 and 11 constitutes strong evidence for the operation of corner-cutting tunneling even when the KIE value is modest. The many-body contributions to these KIEs will be the topic of a forthcoming publication.

The good agreement of the three-body molecular model with several aspects of the experimental data gives us some confidence that it provides a realistic description of the potential energy function in the regions near the saddle point and critical configurations. (One should, of course, not interpret the potential function quantitatively in other regions.)

6. Conclusions

From the dynamics modeling carried out in this work, we believe the following conclusions can be drawn.

(1) It is possible to model several important aspects of ion transfer reactions of complicated, polyatomic substances in solution by three-body potential functions. Such functions can be parameterized by trial-and-error fitting to experimental results combined with simple physically motivated analytic potential functions.

(2) In spite of its classical origins, phenomenological Marcus theory can give an excellent account of quantum-corrected results, even those dominated by multidimensional tunneling processes.

(3) Rate constants for hydride transfer between NAD^+ analogues can be successfully modeled in considerable quantitative detail by variational transition-state theory calculations in which most of the molecular transformations occur by corner-cutting tunneling processes. The most probable critical configurations have C–C distances significantly larger (>0.1 Å) than the C–C distances at the saddle points.

(4) The tightness parameter, τ, correlates with the critical configuration C–C distance. It is a valid qualitative indicator of critical configuration tightness, although it is not quantitatively equal to the sum of the bond orders to the in-flight atom.

(5) The Marcus work terms, W^r and W^p, are not identifiable with any specific feature of the potential energy surface. Neither in the present work nor in our earlier work[4] are there any structures which can be identified as precursor configurations. W^r and W^p represent parts of the standard free energies of activation that do not correlate with the standard free energies of reaction.

Acknowledgment. The authors are grateful to Tomi Joseph, Thanh Truong, Gillian Lynch, and Da-hong Lu for assistance with the computations.

Registry No. D, 7782-39-0.

Gas-Phase Structure and Conformations of Malonyl Difluoride ($COF-CH_2-COF$) and Difluoromalonyl Difluoride ($COF-CF_2-COF$). An Electron Diffraction and ab Initio Study

AnDing Jin,[1a] Hans-Georg Mack,[1b] Alfred Waterfeld,[1c] and Heinz Oberhammer*,[1b]

Contribution from the Institut für Physikalische und Theoretische Chemie, Universität Tübingen, 7400 Tübingen, Germany, and Lehrstuhl für Anorganische Chemie II, Ruhr—Universität Bochum, 4630 Bochum, Germany. *Received March 25, 1991*

Abstract: The geometric structures and conformational compositions of malonyl difluoride, $COF-CH_2-COF$ (1), and difluoromalonyl difluoride, $COF-CF_2-COF$ (2), were studied by gas electron diffraction and ab initio calculations (HF/3-21G and HF/6-31G**). The experimental scattering intensities of both compounds are reproduced best by mixtures of two conformers with aplanar skeletons and the C=O bonds eclipsed with respect to vicinal single bonds (C—C, C—H or C—F). The main conformer of **1** possesses C_1 symmetry with one COF group rotated by $\delta_1(CCCO) = 112\ (2)°$ and the other COF group lying in the CCC plane ($\delta_2(CCCO) = 0°$, i.e. C=O cis to C—C). The presence of a small amount (10 (10)%) of a second conformer with C_2 symmetry and with both C=O bonds eclipsing the C—H bonds is likely. The relative stabilities of the two conformers of **2** are reversed. The low-energy form possesses C_2 symmetry with both COF groups rotated by 120 (2)°, and the high-energy form (30 (15)%) possesses C_1 symmetry with one C=O bond eclipsing one vicinal C—F bond and the other C=O bond eclipsing the opposite C—C bond. The ab initio calculations predict the experimentally determined conformations with C_1 and C_2 symmetry to be stable structures, and their relative stabilities depend on the size of the basis set. The large basis set predicts the correct relative energies for **1** and the small basis set for **2**. Experimental bond lengths and bond angles are reproduced very well by the HF/3-21G method.

Introduction

Over many years the keto–enol tautomerism, conformational properties, and structures of β-dicarbonyl compounds of the type $COX-CH_2-COX'$ have attracted considerable interest by experimentalists and theoreticians. A comprehensive review of these physical properties was given by Emsley.[2] In almost all β-dicarbonyls the U-cis enol form predominates, which is stabilized by intramolecular hydrogen bonding. Structures with asymmetric (C_s symmetry) or symmetric hydrogen bonds (C_{2v} symmetry) are considered in the literature. Assuming planarity of the carbon–oxygen framework of the keto tautomer, three conformations are discussed: U-cis (*Z*,*Z*), W-trans (*E*,*E*), and S-trans (*E*,*Z*).

A considerable number of structural investigations of β-dicarbonyl compounds in the gas phase and in the crystal have been reported in the literature. The parent compound, malondialdehyde (MDA), with X = X' = H, was studied by microwave spectroscopy,[3] resulting in a planar enol U-cis structure of C_s symmetry with a double minimum potential for the O–H···O hydrogen bond. This result has been reproduced by a number of theoretical calculations at various levels of sophistication.[4-7] Gas electron

(1) (a) On leave of absence from Nanjing Normal University. (b) Tübingen. (c) Bochum.

(2) Emsley, J. *Structure and Bonding*: Springer: Berlin 1984; Vol. 57, p 147.

(3) Baughcum, S. L.; Duerst, R. W.; Rowe, W. F.; Smith, Z.; Wilson, E. B. *J. Am. Chem. Soc.* **1981**, *103*, 6296. Baughcum, S. L.; Smith, Z.; Wilson, E. B.; Duerst, R. W. *J. Am. Chem. Soc.* **1984**, *106*, 2260. Turner, P.; Baughcum, S. L.; Coy, S. L.; Smith, Z. *J. Am. Chem. Soc.* **1984**, *106*, 2265.

0002-7863/91/1513-7847$02.50/0